Estuarine, Coastal and Shelf Science 332 (2026) 109766

Contents lists available at ScienceDirect

Estuarine, Coastal and Shelf Science

journal homepage: www.elsevier.com/locate/ecss

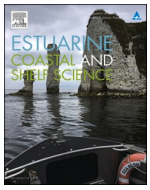

Groundwater-derived nutrient fluxes and offshore mixing rates along the New Jersey coast

Joanna A. Guldin, Charles A. Schutte, Lauren E. Kipp *

Department of Environmental Science, Rowan University, Glassboro, NJ, 08085, USA

ARTICLE INFO

Keywords:
Radium
Nutrients
Groundwater
Coastal mixing
Upwelling

ABSTRACT

Groundwater discharge to the coastal ocean is a vital source of nutrients and trace metals that support photosynthetic life. This study uses radium isotopes as tracers to calculate coastal mixing rates during upwelling and steady state conditions and to quantify the groundwater-derived nutrient flux to the ocean along the southern New Jersey coast. Our best estimate for the coastal mixing rate (apparent horizontal eddy diffusivity) was 18 $km^2\,d^{-1}$ (possible range of 11 – 38 $km^2\,d^{-1}$) based on ^{224}Ra. A box model was used to determine that the flux of groundwater discharge to the coastal ocean is $5.4 \times 10^7\,m^3\,d^{-1}$, with a possible range of 2.8×10^7 – $1.4 \times 10^8\,m^3\,d^{-1}$. The Ra-derived estimate of submarine groundwater discharge was combined with groundwater nutrient concentrations to determine nutrient fluxes of $5.8 \times 10^5\,mol\,d^{-1}$ for nitrate + nitrite (NO_x), $4.3 \times 10^4\,mol\,d^{-1}$ for PO_4, and $2.5 \times 10^4\,mol\,d^{-1}$ for NH_4^+. These results indicate that groundwater discharge is a major source of water and nutrient inputs along the New Jersey coast, similar to the fluxes delivered by the Delaware River and exceeding those delivered by the nearby Mullica River by ~200%. These values serve as baseline estimates for assessing future changes in the magnitude and quality of groundwater discharge driven by human activity and climate change.

1. Introduction

Submarine groundwater discharge (SGD) is defined as any water seeping from land to the coastal ocean after circulating through sediments (Burnett et al., 2003). SGD is a globally significant pathway for freshwater and nutrients to enter coastal ecosystems, exceeding surface water inputs in most reviewed cases (Santos et al., 2021). Therefore, SGD is critical for maintaining coastal ecosystem health and sustainability. Groundwater discharge into coastal waters from fresh- and saltwater interfaces serves as an important source of nutrients and trace metals that support photosynthetic life, thereby supporting local ecosystems and fisheries (Valiela et al., 1990; Moosdorf and Oehler, 2017). Understanding the magnitude of groundwater discharge, as well as the concentration of essential nutrients in groundwater, is crucial for comprehending the scale of groundwater-derived nutrients entering coastal waters.

The flux and quality of groundwater discharging into coastal waters may change in the future due to human activity. Sewage discharge and fertilizer application could increase nutrient additions to the coastal ocean, potentially leading to harmful algal blooms and hypoxia in coastal waters (Paerl, 1997; Diaz and Rosenberg, 2008). Climate change and accelerated groundwater pumping could also impact groundwater quality, as rising sea-levels and excessive extraction may cause saltwater intrusion (Moore and Joye, 2021). This intrusion of saltwater into freshwater aquifers could shift the saltwater-freshwater interface, increasing salinity in groundwater and posing threats to drinking water supplies (Barlow and Reichard, 2010). Increased salinity could mobilize contaminants in groundwater that are more soluble at higher salinities (Sawyer et al., 2016), therefore increasing the flux of elements to coastal waters. SGD may also contribute to coastal hypoxia by delivering byproducts such as sulfide, ammonia, and methane to coastal waters, which can lower dissolved oxygen levels when oxidized (Moore et al., 2024). Given these concerns, studying groundwater chemistry is critical for establishing appropriate pollution management strategies to protect coastal environments and local fisheries.

Coastal mixing rates (cross-shelf eddy diffusivities) describe the rate at which water masses mix in coastal areas, influencing how nutrients and pollutants delivered by SGD are distributed throughout coastal waters. Understanding mixing rates is critical for managing potentially harmful impacts of SGD, as they determine how quickly and widely

* Corresponding author.
E-mail address: kipp@rowan.edu (L.E. Kipp).

https://doi.org/10.1016/j.ecss.2026.109766
Received 18 February 2025; Received in revised form 20 November 2025; Accepted 6 February 2026
Available online 7 February 2026

these substances are spread. Higher mixing rates can spread SGD inputs more widely, diluting concentrations of nutrients and pollutants, while lower mixing rates can create areas of high nutrient or pollutant concentrations. Thus, coastal mixing rates play a vital role in assessing the extent of nutrient dispersion and its implications for coastal ecosystems. This study location is in a region where rapid and expansive development of offshore wind energy is being planned and implemented (New Jersey Board of Public Utilities, 2020). Future installations of wind turbines could increase localized turbulence and add an anthropogenic source of mixing (Schultze et al., 2020).

Radium is a chemical tracer commonly used to study the magnitude of groundwater discharge and the transport of nutrients to the coastal ocean (Burnett et al., 2008). It is a naturally occurring radioactive isotope produced through the decay of thorium isotopes in sediments and is soluble in seawater, meaning groundwater becomes enriched in radium as it resides in an aquifer or when seawater recirculates through sediments. Radium isotopes serve as valuable tools for quantifying groundwater flux and nutrient transport, as direct measurements of these fluxes (e.g. by flow meters) are often challenging (Rama and Moore, 1996). The four radium isotopes decay at different rates, determined by their half-lives ($t_{1/2}$; ^{223}Ra, $t_{1/2} = 11.4$ days; ^{224}Ra, $t_{1/2} = 3.66$ days; ^{226}Ra, $t_{1/2} = 1600$ years; and ^{228}Ra, $t_{1/2} = 5.75$ years), and therefore integrate changes over a range of space- and time-scales. The short-lived isotopes, ^{223}Ra and ^{224}Ra, are particularly useful for calculating coastal mixing rates since these isotopes decay on timescales of days.

The rate and distribution of SGD are influenced by the composition of shelf sediments and whether a coastline lies on an active or passive margin (Santos et al., 2021). This study takes place along the New Jersey coast, a passive margin characterized by a broad, shallow shelf with low topographic relief and sandy sediments. Given its structural similarities to other passive margin coastlines, the New Jersey shelf is representative of passive margin coastal environments. Thus, SGD processes observed here are likely comparable to those in similar regions globally. With New Jersey and other similar passive margin coastlines projected to undergo extensive wind farm development, establishing baseline estimates of SGD is critical. These baselines will serve as a reference point for future studies, enabling direct comparisons of SGD before and after wind energy infrastructure is implemented and providing insight into how other coastal regions may respond to offshore wind development in

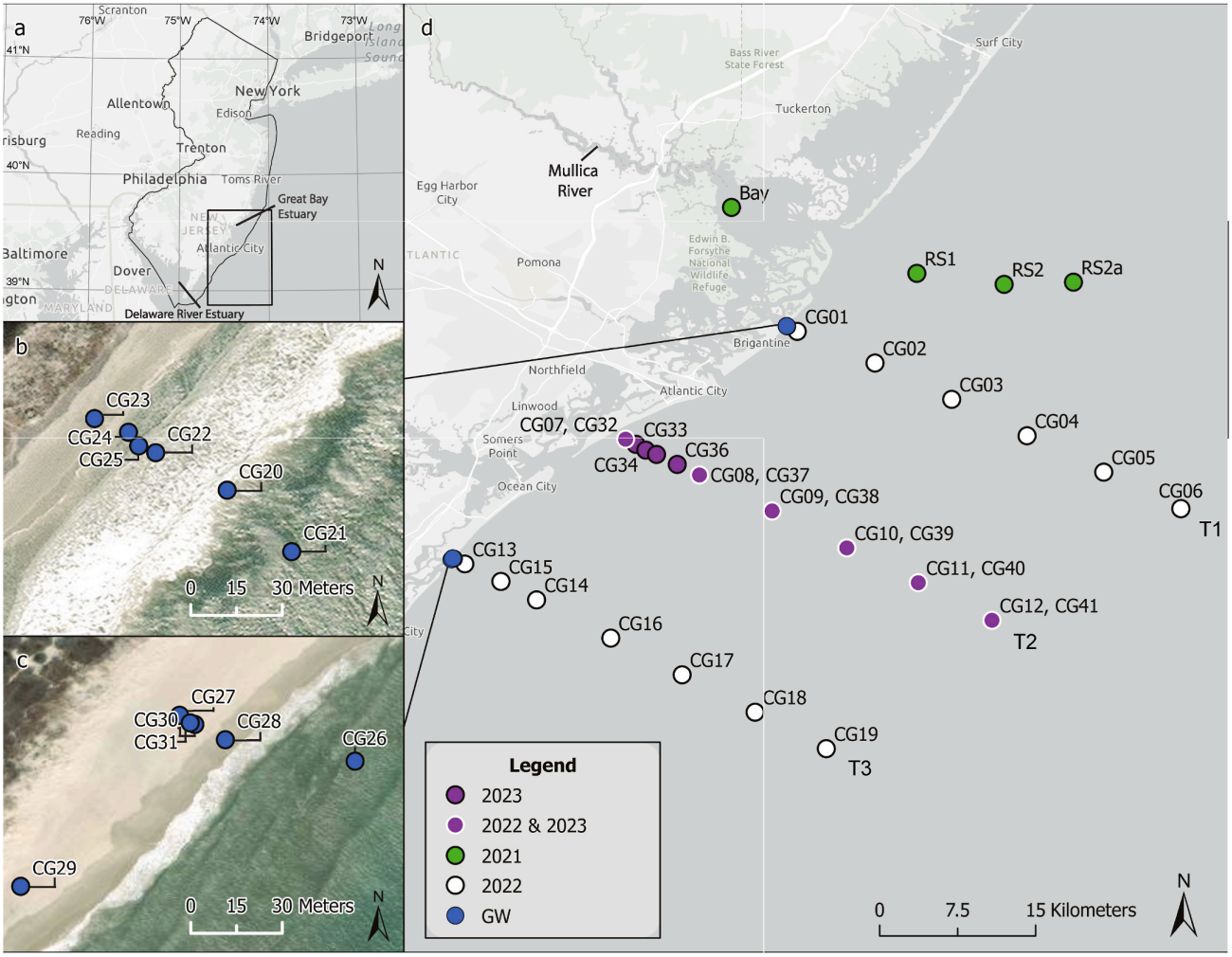

Fig. 1. a) Map of New Jersey showing the study location (black box). b) Groundwater sampling sites at Brigantine beach. c) Groundwater sampling sites at Corson's Inlet State Park. d) Map of the New Jersey coast showing the locations of the groundwater sampling sites (blue circles) and offshore transects. The green circles represent sample collection sites from December 2021, the white circles represent sample collection sites from August 2022, the purple circles represent sample collection sites from June 2023, and the purple circles with white outline represent sites from 2022 and 2023.

coming decades.

In this study, radium and nutrient samples were collected from groundwater and surface waters along the southern New Jersey coast to quantify coastal mixing rates and groundwater-derived nutrient fluxes and assess the hypothesis that groundwater is a significant nutrient source to the coastal ocean in this region. This study represents the first estimates of nutrient fluxes off the southern New Jersey coast, providing baseline values that can be used to assess future changes driven by human activity, climate change, and offshore wind energy development, which is an area of particular interest in SGD research (Santos et al., 2021). Further, this study captures periods of both steady-state conditions and upwelling, addressing the temporal changes in the persistence of groundwater-derived nutrients and allowing us to assess the utility of radium as tracers of coastal mixing and groundwater discharge.

2. Methods

2.1. Study area

Surface water samples were collected along three transects off the coast of Brigantine Beach, Margate City Beach, and Corson's Inlet State Park in southern New Jersey, USA (T1, T2, and T3, respectively; Fig. 1). The transects crossed the shallow shelf, which has sandy sediments and low topographic relief similar to other passive margins along the East Coast of the United States. Samples were collected along the transects at 0.5, 4, 7.5, 11, 14.5, and 18 nautical miles (nm) (0.9, 7.4, 13.8, 20.3, 26.8, and 33.3 km) offshore between August 1, 2022 and August 3, 2022 on the *R/V Petrel.* Six samples were collected on each transect, except for T2, where one additional sample (CG15) was collected at 2.5 nm (4.1 km). T2 was repeated between 13 and 15 June 2023, with higher sampling resolution closer to shore (0.5, 1, 1.5, 2, 3, 4 nm; 0.9, 1.8, 2.7, 3.7, 5.5 km) for a total of 10 samples along the transect.

Groundwater sampling was conducted at Brigantine Beach and Corson's Inlet, the endpoints of T1 and T3. Samples CG20 to CG25 were collected from Brigantine Beach on August 4, 2022, and samples CG26 to CG31 were collected from Corson's Inlet on August 5, 2022. Samples were collected at varying depths in the sand (0.15-2.64 m) and distances from the surf (15-83 m) to find variation in salinity (0.71-32.7) because ionic strength can influence particle reactivity and complexation of solutes like radium and nutrients. One surface water sample was collected by wading into the surf zone at each sampling site (CG21 & CG26).

Surface water samples were also collected north of T1 on December 14, 2021. One sample was collected within Great Bay Estuary, and three samples were collected along a transect offshore Jacques Cousteau National Estuarine Reserve, at the mouth of the estuary. Although these samples did not overlap with the other transects, they captured the outflow of the Mullica River (Fig. 1) and provide an additional year for comparison.

2.2. Offshore sample collection

Surface water samples (100L) were collected into plastic barrels from 2 m using a submersible pump (Tsurumi). The water was filtered through 1.5" diameter sample cartridges packed with ~20 g of manganese oxide (MnO_2)-coated acrylic fiber at ~1 L min^{-1} to quantitatively scavenge the radium from the seawater (Reid et al., 1979). In 2021, only 20 L of surface water was collected using a peristaltic pump (Solinst) and was gravity filtered (<1 L min^{-1}).

A Castaway-CTD (YSI) was used to profile temperature and salinity at each station. A handheld YSI sensor was used to collect additional discrete measurements of temperature and salinity in surface water at each station.

2.3. Groundwater sample collection

Groundwater samples were collected by connecting a peristaltic pump with a drive point piezometer (Solinst) inserted deep enough beneath the beach surface to pull groundwater without creating air bubbles. Radium samples were pumped into a 20 L cubitainer and gravity filtered over a MnO_2 fiber. Groundwater was collected into a 1 L graduated cylinder to measure O_2, pH, temperature, and salinity using YSI sensors.

Groundwater nutrient samples were collected using tubing connected to the peristaltic pump and a sampling syringe, and the tubing and syringe were rinsed 3 times with sample water between every sample. 3 mL of sample was used to rinse a 0.2 μm PES syringe filter prior to collecting the sample in an acid-washed 15 mL centrifuge tube. One blank sample was collected each day of sampling using ultrapure water. All samples were placed in a cooler on ice and frozen until processing and analysis.

2.4. Sample analysis

On shore, fiber samples were measured for ^{223}Ra and ^{224}Ra using a Radium Delayed Coincidence Counter (RaDeCC) system (Moore and Arnold, 1996). Activities were first measured <4 days after collection to determine the short-lived ^{223}Ra and ^{224}Ra. Samples were then counted again 4 and 8 weeks after collection to measure the activities of ^{224}Ra and ^{223}Ra supported by ^{228}Th and ^{227}Ac, respectively. The ^{223}Ra and ^{224}Ra activities reported below are in excess of the measured parent isotopes. Fiber standards spiked with ^{232}Th with daughters in equilibrium were measured twice a week within the 8-week period to calculate detector efficiencies for the measurement of ^{224}Ra. The efficiency of ^{223}Ra measurements was calculated based on the ^{224}Ra efficiency, as described in Moore and Cai (2013). Efficiencies for the two detectors used were 43.4% and 53.4% for ^{224}Ra and 25.0% and 30.8% for ^{223}Ra. Detector blanks were determined by running detectors with no sample holders collected (yielding a "lab air" blank) or with empty sample holders; the average of both run types across both detectors used was considered the blank value. For ^{223}Ra, the blank activity was zero. For ^{224}Ra, the average blank was 0.013 counts per minute; multiplying this by 3 and converting to units of dpm 100 L^{-1} yields a detection limit of ~0.44 dpm 100 L^{-1} for 20 L groundwater samples and ~0.09 dpm 100 L^{-1} for 100 L surface water samples. Error values on RaDeCC measurements are calculated as 1 divided by the number of decay events recorded.

Fiber samples were subsequently combusted in a muffle furnace at 820 °C for 16 h. The resulting ash was then packed into polystyrene test tubes, sealed with epoxy to prevent gas exchange. After waiting at least three weeks for daughter isotopes to reach equilibrium, samples were measured for ^{228}Ra and ^{226}Ra using a 16 mm well-type small anode germanium crystal (SAGe) gamma detector. ^{228}Ra was counted using lines of ^{228}Ac (338 and 911 keV), and ^{226}Ra was counted using lines of ^{214}Pb (352 keV). Ashed fiber standards, prepared using a standard solution containing ^{226}Ra and ^{232}Th with daughter isotopes in equilibrium, were measured to determine detector efficiencies. Gamma detector blanks were determined by running the detector with blank ashed fiber (fiber that has not been in contact with surface or groundwater) for ~7 days. Any measurable activities recorded in the 338, 352, and 911 keV channels were subtracted from the measured sample activities at those photopeaks. Error values on final activities are propagated 1-sigma errors from both the blank and sample runs.

Water samples were analyzed for nitrate + nitrite (NO_x), PO_4, and NH_4^+ on a Seal Analytical AQ300 discrete nutrient analyzer using colorimetric methods, which have detection limits of 0.00021 mol m^{-3}, 0.000065 mol m^{-3}, and 0.000428 mol m^{-3} (Methods for Determination USEPA Method 353.2, 365.1, 350.1, respectively, 1993).

3. Results

3.1. Hydrography along transects

The water column was stratified at the time of sampling in 2022 and 2023, with temperatures ranging from 25.4 °C at the surface to 10.5 °C at depth in 2022 and 19.1 °C to 12.1 °C in 2023 (Fig. 2). The isopycnals sloped down slightly in 2022, with warmer water reaching greater depths offshore. In 2023, the temperature gradient was not as strong. Surface waters were colder at the time of sampling in 2023 because sampling occurred earlier in the season in 2023 (June) compared to 2022 (August). The depth of the mixed layer was approximately 6.5 m, determined based on the average MLD recorded on the temperature profiles. Here, we defined stratification based on temperature, since the isopycnals closely follow the temperature distribution (Fig. 2).

3.2. Radium activities and nutrient concentrations in groundwater

The radium activities and nutrient concentrations in groundwater did not have a strong relationship with salinity across the two beaches sampled (Supplementary Fig. 1). The absolute activities of radium ranged from 0.28 to 29 dpm 100 L^{-1} for ^{223}Ra, 5.2 to 335 dpm 100 L^{-1} for ^{224}Ra, 0.14 to 60 dpm 100 L^{-1} for ^{226}Ra, and 3.1 to 173 dpm 100 L^{-1} for ^{228}Ra. The lowest activities were in the freshest sample (salinity 0.71), consistent with low Ra solubility at low ionic strength (Krishnaswami et al., 1982). Nutrient concentrations varied from 0.0012 to 0.0388 mol m^{-3} for NO_x, 0.0008 to 0.0023 mol m^{-3} for PO_4, and 0 to 0.0015 mol m^{-3} for NH_4^+. One outlier was excluded from the analysis of NO_x (CG22, 0.0988 mol m^{-3}) and the analysis of NH_4^+ (CG31, 0.0069 mol m^{-3}). Since there was no clear gradient between the freshwater endmember and seawater, average radium activities, radium activity ratios, and nutrient concentrations were calculated to serve as the groundwater endmembers (Table 1).

Table 1
Average radium activities and nutrient concentrations in groundwater.

^{223}Ra (dpm 100L^{-1})	11 ± 8
^{224}Ra (dpm 100L^{-1})	134 ± 91
^{226}Ra (dpm 100L^{-1})	21 ± 15
^{228}Ra (dpm 100L^{-1})	73 ± 48
^{224}Ra/^{228}Ra	1.9 ± 0.8
NO_x (mol m^{-3})	0.0164 ± 0.0149
PO_4 (mol m^{-3})	0.0014 ± 0.0005
NH_4^+ (mol m^{-3})	0.0007 ± 0.0006

3.3. Radium activities and nutrient concentrations in seawater

The activities of short-lived radium isotopes ^{223}Ra and ^{224}Ra were higher and measurable near the coast and decreased exponentially with distance due to radioactive decay and dilution. In 2022, activities of ^{223}Ra and ^{224}Ra >20 km offshore were <0.17 dpm 100 L^{-1} and <0.25 dpm 100 L^{-1}, respectively. Near the coast (<15 km offshore), ^{223}Ra activities averaged 0.93 ± 0.59 dpm 100 L^{-1} in 2021, 0.52 ± 0.63 dpm 100 L^{-1} in 2022, and 0.52 ± 0.13 dpm 100 L^{-1} in 2023 (Fig. 3a). For ^{224}Ra, activities near the coast averaged 8.8 ± 4.8 dpm 100 L^{-1} in 2021, 5.5 ± 7.2 dpm 100 L^{-1} in 2022, and 6.1 ± 1.4 dpm 100 L^{-1} in 2023 (Fig. 3c).

The activities of long-lived isotopes ^{226}Ra and ^{228}Ra decreased between 0 and 10 km in 2022, followed by a slight increase offshore. In 2023, the activities remained relatively constant. In 2021, a decrease was observed between the bay and nearest seawater sample, followed by the same slight increase offshore as observed in 2022. The ^{226}Ra activities measured near the coast averaged 9.9 ± 2.0 dpm 100 L^{-1} in 2021, 6.5 ± 4.0 dpm 100 L^{-1} in 2022, and 10 ± 1.0 dpm 100 L^{-1} in 2023 (Fig. 3b). For ^{228}Ra, activities near the coast averaged 18 ± 1.7 dpm 100 L^{-1} in 2021, 15 ± 10 dpm 100 L^{-1} in 2022, and 23 ± 1.3 dpm 100 L^{-1} in 2023 (Fig. 3d).

Nutrient concentrations in seawater were comparable between 2022 and 2023. Average NO_x and PO_4 concentrations were 0.0007 ± 0.0001 mol m^{-3} and 0.0001 ± 0.00002 mol m^{-3} in 2022, and 0.0006 ± 0.0001 mol m^{-3} and 0.0003 ± 0.00005 mol m^{-3} in 2023, respectively. NH_4^+ was below the detection limit in all samples both years.

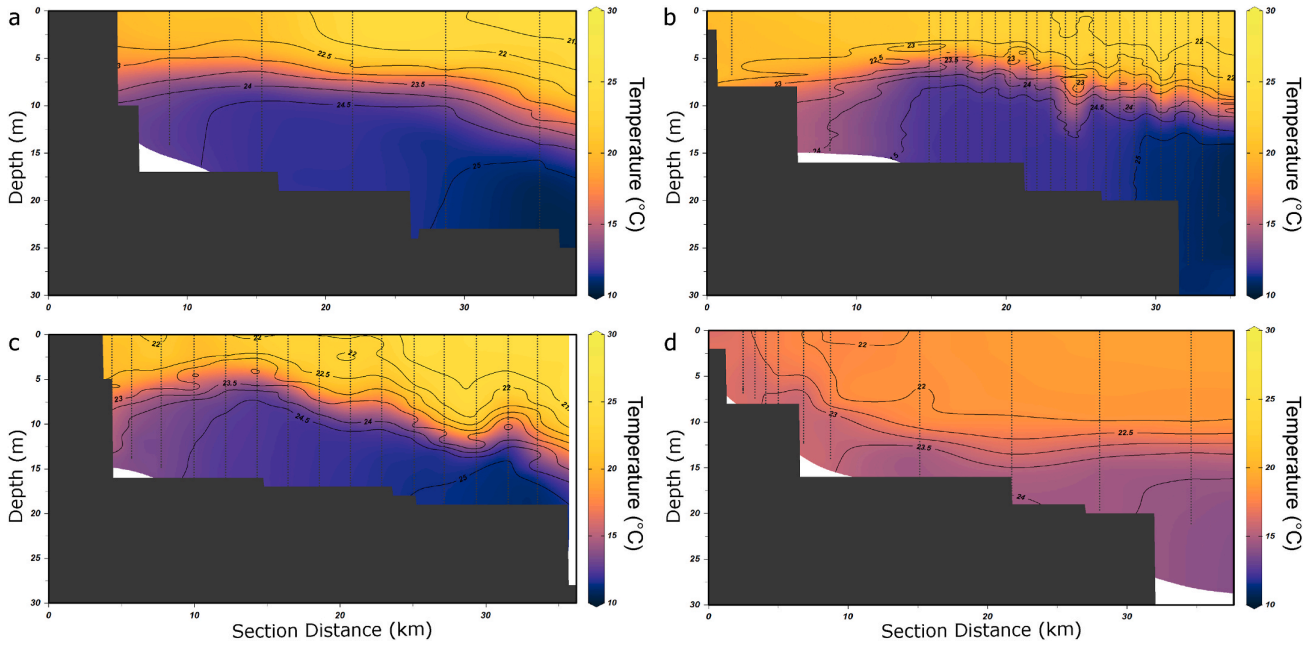

Fig. 2. Sea surface temperatures measured using a CTD-Castaway along a) transect 1 in 2022, b) transect 2 in 2022, c) transect 3 in 2022, and d) transect 2 in 2023.

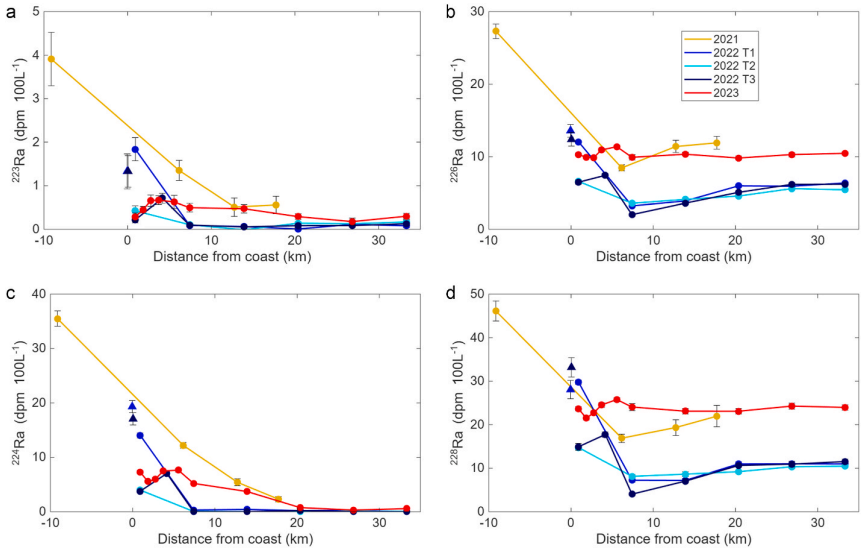

Fig. 3. a) Excess radium-223, b) radium-226, c) excess radium-224, and d) radium-228 measured offshore the southern New Jersey coast in 2021 (yellow), 2022 (blue), and 2023 (red). One sample was collected within the Great Bay Estuary in 2021; this sample is associated with a negative distance from the coast to represent its position in the bay. The samples collected from the surf at Brigantine Beach (CG21) and Corson's Inlet (CG26) are included on transects 1 and 3, respectively (triangles).

4. Discussion

Near shore (<15 km) radium activities in 2021 and 2023 are comparable to previous studies along the east coast. Moore (2000b) reported average near shore activities of 2.0 dpm 100 L^{-1} for ^{223}Ra, 11 dpm 100 L^{-1} for ^{224}Ra, 18 dpm 100 L^{-1} for ^{226}Ra, and 23 dpm 100 L^{-1} for ^{228}Ra between Cape Fear and the Savannah River. Offshore (>15 km) activities in 2021 and 2023 are also comparable to a 2007 study offshore the Great Bay estuary: Stachelhaus et al. (2012) reported activities of ~0.05-0.40 dpm 100 L^{-1} for ^{223}Ra, ~1.2-4.0 dpm 100 L^{-1} for ^{224}Ra, ~8.0-12 dpm 100 L^{-1} for ^{226}Ra, and ~8.5-15 dpm 100 L^{-1} for ^{228}Ra 15 to 35 km offshore, although they note possible background contamination for ^{224}Ra. They found total ^{223}Ra and ^{224}Ra activities leveled off at values of 0.11 dpm 100 L^{-1} and 1.6 dpm 100 L^{-1} at 30 km offshore, respectively. In 2023, we found ^{223}Ra and ^{224}Ra activities leveled off around 20 km offshore, at values of ~0.25 dpm 100 L^{-1} and ~0.53 dpm 100 L^{-1}, respectively.

Radium activities were lowest in 2022, a trend consistent across all measured isotopes, both short-lived and long-lived. Abnormally low radium activities in 2022 indicates that there may not have been steady state conditions at the time of sampling. Typical activities in the Atlantic Ocean are ~4 dpm 100 L^{-1} for ^{228}Ra and ~7.5 dpm 100 L^{-1} for ^{226}Ra (e.g. Key et al., 1985; Charette et al., 2015); we expect nearshore activities of these isotopes to be notably higher (e.g. ~10-30 dpm 100 L^{-1} for ^{228}Ra, ~10-20 dpm 100 L^{-1} for ^{226}Ra; Moore, 2000b). Nearshore (0.5 nm) activities on T1 (2022) were elevated compared to the other 2022 transects and compared to T2 in 2023 (particularly for the short-lived isotopes); this is likely due to outflow from the Mullica River and Great Bay Estuary, where high activities were detected for all isotopes when this region was sampled in 2021.

4.1. Potential upwelling event in 2022

Surface water chemistry in 2022 may have been impacted by an upwelling event. Upwelling is common along the southern New Jersey coast and is well documented, with the continental shelf adjacent to

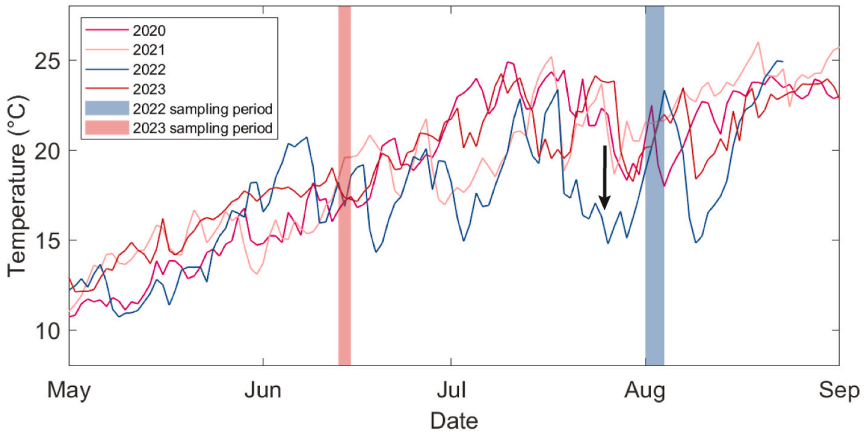

Fig. 4. Daily average sea surface temperatures in 2020 (hot pink), 2021 (light pink), 2022 (blue), and 2023 (red). The blue rectangle represents the sampling period in 2022 (August 3-5), and the red rectangle represents the sampling period in 2023 (June 13-15). The arrow demonstrates the difference in SST in 2022 compared to other years. Data was collected from NOAA station ACYN4 located at Atlantic City (NOAA's National Ocean Service).

Great Bay being a known upwelling center (Glenn et al., 2004). Sea surface temperatures near Atlantic City were significantly lower during the last two weeks of July in 2022 than they were in 2020, 2021, and 2023 (Fig. 4). This indicates that there may have been an upwelling event that carried cold, deeper water up to the surface about a week prior to sampling and pushed warmer surface waters offshore. Near-bottom waters are typically enriched in radium due to the proximity to the sediment source of this element, though the dominantly sandy sediments in our study area typically have lower fluxes of radium than finer grained sediments (Moore et al., 2008). If groundwater from the beach face is the primary source of Ra to the coastal zone (rather than diffusion from sediments), it is possible that the upwelling event pushed surface waters with higher (groundwater-derived) Ra activities offshore and replaced them with lower activity waters from below. Although the water column had restratified at the time of our sampling (Figs. 2 and 4), it would take at least 3 weeks for the system to reach steady state again (~6 half-lives of ^{224}Ra), thus Ra activities would remain low even after surface water temperatures warmed.

It is also possible that upwelling of nutrient-rich deep waters triggered a phytoplankton bloom. Although Ra is not biologically utilized, there is some evidence of coincidental uptake due to the similar ionic radii and valence configurations of Ra and silica and barium (e.g. van Beek et al., 2022). Diatoms, which build silicate tests, are the dominant phytoplankton taxa in our study area during upwelling events (Moline et al., 2004). A large diatom bloom and/or a change in phytoplankton community structure triggered by the upwelling event could therefore result in decreased levels of Ra isotopes resulting from coincidental Ra uptake in place of silica. Chlorophyll concentrations offshore Atlantic City do not show high productivity during that period (NASA/MODIS; Supplementary Fig. 2); however, MODIS presents chlorophyll data as an 8-day average, thus it is possible that short-lived blooms may not have been fully captured.

Low radium activities and sea surface temperatures provide evidence that there may not have been steady state conditions at the time of sampling in 2022. In the weeks prior to sampling in 2023, however, sea surface temperatures were comparable to other years of data. Coastal mixing rates and groundwater fluxes were calculated using both years of data to determine how an upwelling event may affect these estimations.

4.2. Coastal mixing rates

Coastal mixing rates were determined by calculating the apparent horizontal eddy diffusion coefficient. The distribution of radium isotopes in coastal waters is influenced by both advection and diffusion; however, here we focus on the offshore component of mixing (perpendicular to the coastline) and assume that alongshore advection is not significant compared to eddy diffusion in influencing changes in nearshore radium activities with distance from the coast. Since advection in this area is primarily directed north to south (alongshore) rather than east to west (offshore), we can isolate diffusion driven mixing rates moving offshore. If offshore advection is indeed significant, its effects will be included in the calculated horizontal eddy diffusivity (K_h) term, thus we consider our result an "apparent" horizontal eddy diffusivity coefficient (Huh and Ku, 1998).

Mixing rates were estimated using short-lived radium isotopes ^{223}Ra and ^{224}Ra. Since these isotopes decay on timescales of days, a decay term must be present in the mixing equation to account for their rapid decrease in concentration over time (Moore, 2000b). The relationship between activity and distance from coast was used to calculate the horizontal eddy diffusivity coefficient (K_h) (Fig. 5), following equation (1) below:

$$K_h = \frac{\lambda}{m^2} \quad (1)$$

where λ is the decay constant of ^{223}Ra or ^{224}Ra (0.0608 and 0.1894 d^{-1}, respectively) and m is the slope of the line fit. In 2022, the slope for ^{223}Ra was −0.059 (possible range of −0.102 to −0.015), resulting in a K_h value of 17 $km^2\,d^{-1}$ and a possible range of 5 – 244 $km^2\,d^{-1}$. In 2023, the slope for ^{223}Ra was −0.026 (possible range of −0.049 to −0.0025), resulting in a K_h value of 91 $km^2\,d^{-1}$ and a possible range of 25 – 9800 $km^2\,d^{-1}$. For ^{224}Ra the slope was −0.159 (−0.241 to −0.076) in 2022 and -0.10 (−0.13 to −0.070) in 2023, resulting in K_h values of 7 $km^2\,d^{-1}$ (3 – 32 $km^2\,d^{-1}$) and 18 $km^2\,d^{-1}$ (11 – 38 $km^2\,d^{-1}$), respectively. Ranges are based on the 95% confidence interval of the line fit. The upper limit using ^{223}Ra is not reasonable and is driven by a poor line fit to the data. Our analysis was influenced by low ^{223}Ra activities, which were close to the detection limit in both years.

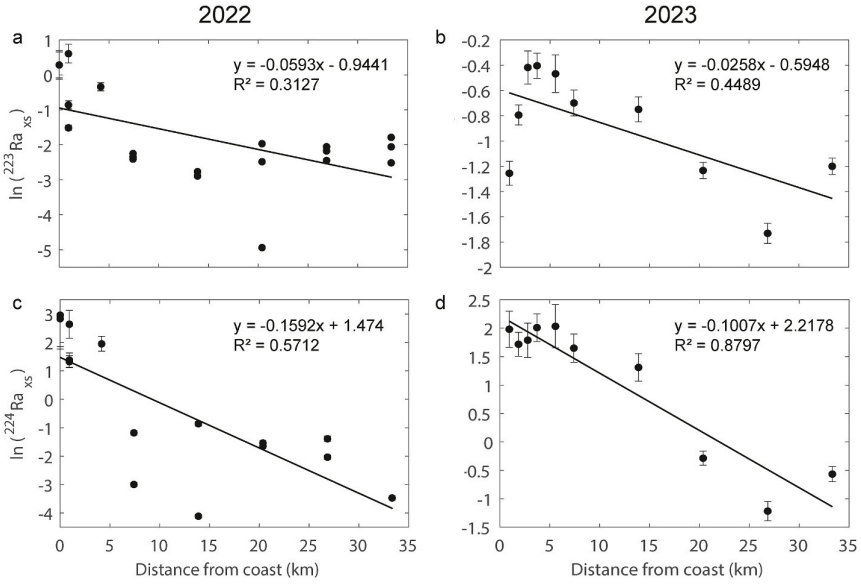

Fig. 5. The decay of radium-223 in a) 2022 and b) 2023 and radium-224 in c) 2022 and d) 2023 plotted with distance from coast. The black solid line indicates the line fit, and the slope of the line fit and the R^2 values are presented on the respective figures.

The coastal mixing rate estimated using steady-state ^{224}Ra data is more accurate (based on a better line fit) and aligns well with previous studies. Stachelhaus et al. (2012) reported rates of 14.69 – 19.01 km^2 d^{-1} offshore the Great Bay estuary, and Moore (2000b) reported a rate of 36.2 km^2 d^{-1} off the coast of South Carolina. Conversely, the 2023 mixing rate we estimated using ^{223}Ra is higher than that found by Stachelhaus et al. (2012) and Moore (2000b), who found rates of 0.86 – 13.82 km^2 d^{-1} and 31.5 km^2 d^{-1}, respectively.

The coastal mixing rates estimated from data collected after the presumed upwelling event in 2022 are lower than those from steady state conditions in 2023, due to the lower radium activities observed offshore in 2022. The low radium activities appear to reach a minimum around 15-20 km; if we calculate the mixing rate from the coast to this boundary, the apparent K_h is even lower. These estimates reflect the aftermath of upwelling, when the surface box had not yet returned to steady state. Thus, these results indicate that upwelling events may result in lower apparent coastal mixing rates that are unlikely to represent steady state conditions. This emphasizes the importance of understanding temporal variability in groundwater-derived nutrient persistence, as nutrients from this source may not persist as long in regions with regular perturbations like upwelling.

4.3. Nearshore water residence times

Water residence times on the shelf were estimated using the ^{224}Ra/^{228}Ra radium isotope ratio and the age model equation derived in Moore (2000a):

$$\left[\frac{224Ra}{ex\ 228Ra}\right]_{obs} = \left[\frac{224Ra}{ex\ 228Ra}\right]_{i} e^{-\lambda 224 t} \quad (2)$$

where the observed (obs) ratio is radium activity in each surface water sample, the initial (i) ratio is the average radium activity in groundwater, λ is the decay constant in days, and t is the residence time. Using the ratio of the isotopes corrects for the effects of mixing and dilution, such that any change in the ratio can be attributed to decay. The above equation assumes that the ratio will eventually decrease to zero as time increases, but this is not the case for ^{228}Ra, since the open ocean contains measurable levels of unsupported ^{228}Ra (Moore, 2000a). Therefore, we use excess (ex) above open ocean background values for ^{228}Ra. Since typical ^{228}Ra activities in the Atlantic Ocean are ~4 dpm 100 L^{-1} (Key et al., 1985; Charette et al., 2015), this value was subtracted from our sample activities to determine excess ^{228}Ra supplied from groundwater. The initial ratio (i) was 1.9 ± 0.8, based on the average groundwater value (Table 1).

Around 20 km offshore, short-lived radium activities appear to reach an asymptote (Fig. 3); this was set as the boundary of our coastal box (see Section 4.4. below) thus the samples collected at the stations beyond this 20 km boundary were not used to calculate residence times.

Our best estimates of nearshore water residence times based on the ^{224}Ra/^{228}Ra ratio are 14.7 days (possible range of 11.7 to 16.5 days) for 2022 and 11.1 days (possible range of 8.1 to 13.0 days) for 2023. These ranges are based on the standard deviation of the groundwater end-member. The longer residence time calculated for 2022 resulted from low average short-lived isotope activities in the surface box. This does not indicate lower groundwater inputs in 2022; rather, upwelling likely transported the groundwater signal out of the surface box. These differences highlight the temporal variability in residence time estimates driven by physical processes like upwelling.

The documented upwelling event in 2022 violates the assumption of steady state, thus the residence time calculated for this year is likely an over-estimate. However, we use this value to calculate groundwater discharge in 2022 to demonstrate how upwelling may impact groundwater flux estimates (Section 4.4). The residence time calculated for 2023 is more representative of steady state conditions and provides a better baseline for typical residence times in this region.

4.4. Flux of ^{223}Ra, ^{224}Ra, ^{226}Ra, and ^{228}Ra from submarine groundwater discharge

Submarine groundwater discharge fluxes were estimated using a box model approach. The activity of radium in the coastal water is assumed to be in steady state, with the sources of radium being advection onshore, river discharge, and groundwater discharge, and the sinks being advection offshore and loss to radioactive decay (Eqn. (3)):

$$[Ra]_{off} * V * k + F_{riv}[Ra]_{riv} + F_{gw}[Ra]_{gw} = [Ra]_{surf} * \lambda * V + [Ra]_{surf} * V * k \quad (3)$$

In the above equation, $[Ra]_{off}$ is the radium activity offshore (atoms m^{-3}), V is the water volume in the box (m^3), k is the inverse of the water residence time (d^{-1}), F_{riv} is the discharge of the Mullica River (m^3 d^{-1}), $[Ra]_{riv}$ is the radium activity measured in Great Bay in 2021 (atoms m^{-3}), F_{gw} is the input of radium from groundwater (m^3 d^{-1}), $[Ra]_{gw}$ is the average radium activity in groundwater (atoms m^{-3}), $[Ra]_{surf}$ is the radium activity in surface water in the coastal box (atoms m^{-3}), and λ is the decay constant of ^{223}Ra, ^{224}Ra, ^{226}Ra, or ^{228}Ra (d^{-1}). In this analysis, the model is limited to the surface mixed layer since the water column was stratified at the time of sampling (Fig. 2d), thus the benthic sediment source of Ra is ignored. The following equation was derived from Eqn. (3) to solve for F_{gw} (Eqn. (4)):

$$F_{gw} = \left(\left([Ra]_{surf} * \lambda * V + \left([Ra]_{surf} - [Ra]_{off}\right) * V * k\right)\right) - \left([Ra]_{riv} * F_{riv}\right) \ / \ [Ra]_{gw} \quad (4)$$

where the radium activity offshore is assumed to be 0 for ^{223}Ra and ^{224}Ra, 7.5 dpm 100 L^{-1} for ^{226}Ra, and 4 dpm 100 L^{-1} for ^{228}Ra. Here, F_{riv} is the average Mullica River discharge measured between 1 and 3 August 2022 (7.3×10^4 m^3 d^{-1}) and on 13 and June 15, 2023 (9.3×10^4 m^3 d^{-1}) (USGS).

The water volume was determined by dividing the surface box into six boxes in 2022 and eight boxes in 2023, with each box spanning the width of all three transects and containing at least one of the collected samples (sampling resolution was higher in 2023). The volume of each box was then calculated using the average depth of the mixed layer measured along transect 2 in 2023 (6.5 m), the distance between transects 1 and 3 (35 km), and the width of each box (determined by the midpoint between two sample collection sites). Inventory ($[Ra]_{surf}$ *V) was then calculated for each individual box, and the inventories were summed to determine the final inventory of the surface box.

Since the 2022 transects show that the Ra activities are generally consistent over this length of coastline, we assume that our single transect from 2023 is representative of the whole box.

Due to its comparatively low water discharge flux, the Mullica River is not a major source of radium inputs to the surface box. To test the sensitivity of the model to inputs from the Mullica River, we removed $[Ra]_{riv}$*F_{riv} from Eqn. (3); removing this source resulted in only a 0.11%, 0.05%, 0.22%, and 0.06% increase in the groundwater fluxes using ^{223}Ra, ^{224}Ra, ^{226}Ra, and ^{228}Ra, respectively.

Submarine groundwater discharge to the coastal ocean was calculated using the four different isotopes, yielding consistent flux values between each isotope (Table 2). In 2022, groundwater flux could not be calculated using ^{226}Ra because all but three samples were below the background value. The estimated values are on the same order of magnitude between both years of sampling. However, the water flux

Table 2
Groundwater volume fluxes (m^3 d^{-1}) calculated using ^{223}Ra, ^{224}Ra, ^{226}Ra and ^{228}Ra in 2022 and 2023.

	2022	2023
^{223}Ra	1.5×10^7 (8.7×10^6 – 5.5×10^7)	3.0×10^7 (1.7×10^7 – 1.1×10^8)
^{224}Ra	2.2×10^7 (5.9×10^6 – 3.0×10^7)	4.4×10^7 (2.6×10^7 – 1.3×10^8)
^{226}Ra	-	4.7×10^7 (2.7×10^7 – 1.9×10^8)
^{228}Ra	3.2×10^7 (1.9×10^7 – 9.3×10^7)	9.5×10^7 (5.7×10^7 – 2.7×10^8)

calculated in 2022 using the data from the upwelling period is 50%, 49%, and 66% lower than the 2023 flux using ^{223}Ra, ^{224}Ra, and ^{228}Ra, respectively. This does not necessarily indicate a reduction in the actual groundwater discharge but rather an apparent decrease in the groundwater-derived flux due to the loss of radium from surface waters during upwelling. We interpret this as upwelling transporting approximately half the radium offshore (or potentially half the radium being removed during a diatom bloom), leading to lower tracer-based flux estimates. These findings indicate the importance of ensuring steady state conditions when determining groundwater fluxes.

Averaging all flux values from 2023, we determined a water flux of 5.4×10^7 m^3 d^{-1}, with a possible range of 2.8×10^7 to 1.4×10^8 m^3 d^{-1}. Normalized to coastline length, the average groundwater flux is 1.5×10^6 m^3 km^{-1} d^{-1}, with a possible range of 8.0×10^5 to 4.0×10^6 m^3 km^{-1} d^{-1}. These possible ranges are based on the standard deviation on the average radium activity in groundwater and the standard deviation in the water residence time.

These groundwater flux values are comparable to previous studies along the east coast of North America. Moore (2010) reported an average groundwater flux of 9.5×10^5 m^3 km^{-1} d^{-1}, noting that such flux values tend to be consistent regardless of scale, from small bays to 600 km of coastline, from North Carolina to Florida. This supports the conclusions of Santos et al. (2021), who reported consistent SGD rates across different ecosystem types along the east coast, noting that these fluxes were generally smaller than those reported on other coasts globally.

A recent review of Ra isotopes as tracers of SGD by Garcia-Orellana et al. (2021) suggests that the short-lived Ra isotopes are more appropriate for calculating fluxes in nearshore coastal environments, as the time- and space-scales captured by these isotopes are more consistent with the shorter water residence times. Considering only the ^{224}Ra- and ^{223}Ra- based estimates from 2023 results in a groundwater volume flux of 3.7×10^7 m^3 d^{-1}; we use this value to determine the groundwater-derived nutrient fluxes below.

4.5. Groundwater-derived nutrient fluxes

Groundwater-derived fluxes of nitrate and nitrite (NO_x), phosphorus (PO_4), and ammonium (NH_4^+) were estimated by multiplying the nutrient concentration by the volumetric groundwater flux following equation (5) below:

$$\textit{Nutrient flux} = \textit{nutrient concentration x water flux} \quad (5)$$

Santos et al. (2008) calculated a net groundwater nutrient end-member that was adjusted for seawater nutrient concentrations, based on the observation that SGD in their study system was predominately composed of recirculated seawater. As SGD in this study area is also likely dominated by recirculated seawater, the nutrient concentrations used are the average values measured in groundwater (mol m^{-3}) (Table 1) minus the average seawater values measured offshore between 2022 and 2023 (mol m^{-3}) (Santos et al., 2008). Water flux is the average SGD flux derived from ^{223}Ra and ^{224}Ra (3.7×10^7 m^3 d^{-1}).

Table 3
Groundwater-derived nutrient fluxes in comparison to nutrient fluxes estimated from the Mullica and Delaware River (mol d^{-1}).

	Groundwater	Mullica River (at Batsto)	Delaware River (at Trenton)
NO_x	5.8×10^5 (2.8×10^4 – 1.1×10^6)	5.3×10^2 (1.4×10^2 – 9.2×10^2)	1.0×10^6 (9.5×10^5 – 1.2×10^6)
PO_4	4.3×10^4 (2.5×10^4 – 6.0×10^4)	1.5×10^2 (7.9×10^1 – 2.2×10^2)	1.9×10^4 (1.3×10^4 – 2.6×10^4)
NH_4^+	2.5×10^4 (3.2×10^3 – 4.8×10^4)	1.8×10^2 (5.3×10^1 – 3.1×10^2)	2.9×10^4 (1.4×10^4 – 4.3×10^4)

Estimated groundwater-derived nutrient fluxes and the potential ranges (Table 3) are based on the standard deviations of the nutrient concentrations and the range in the groundwater discharge estimate. If nutrient fluxes were calculated for 2022, they would be approximately 50% lower than those from 2023, again highlighting the importance of the steady-state assumption.

Nutrient fluxes from the Mullica River were estimated using a water flux of 9.3×10^4 m^3 d^{-1} (USGS) and mean nutrient concentrations of 0.006 ± 0.001 mol m^{-3}, 0.002 ± 0.001 mol m^{-3}, and 0.002 ± 0.001 mol m^{-3} for NO_x, PO_4, and NH_4^+, respectively (NJDEP Bureau of Marine Water Monitoring, 2020). The water flux reflects the mean discharge recorded at the USGS gauge station in the Mullica River at Batsto on 13 and June 15, 2023, coinciding with offshore sampling. Nutrient concentrations are based on NJDEP buoy (R28) data collected during the summer months (June-Sept.) between 2014 and 2022. These nutrient fluxes are smaller than those estimated from groundwater due to the river's much smaller water flux.

Nutrient fluxes from the Delaware River were estimated using a water flux of 1.2×10^7 m^3 d^{-1} (Delaware River Basin Commission, 2023) and mean nutrient concentrations of 0.090 ± 0.011 mol m^{-3}, 0.002 ± 0.001 mol m^{-3}, and 0.002 ± 0.001 mol m^{-3} for NO_3, PO_4, and NH_4^+, respectively (Fisher & Gustafson, 2019, 2020). The discharge was recorded from the USGS gauge station in the Delaware River at Trenton, the furthest downstream station not tidally influenced. Nutrient concentrations are based on data collected in the river at Trenton during the summer months in 2018 and 2019. These estimates are very conservative because the water flux and nutrient data were collected upstream of major tributaries and estuarine zones where additional nutrient inputs and chemical transformations occur.

These results demonstrate that groundwater is a significant nutrient source to this stretch of the New Jersey coastline, greater than inputs from the Mullica River and similar to those from the Delaware River. SGD:river ratios for the Delaware River were 0.61, 2.7 and 0.86 for NO_x, PO_4, and NH_4^+, respectively. These findings align with global trends reported by Santos et al. (2021), who found SGD:river nutrient flux ratios of 0.1-10 in many cases, indicating that SGD and river inputs are often similar in magnitude across coastal ecosystems.

5. Conclusions

Radium activities in groundwater and surface water were used to determine coastal mixing rates and groundwater fluxes during periods of both upwelling and steady state conditions along the southern New Jersey coast. When the system is in steady state, coastal mixing rates are comparable to other estimates along the US East Coast, whereas data collected during an upwelling event resulted in lower mixing rates and an approximate 55% underestimation of groundwater fluxes compared to steady state conditions, highlighting the need for steady state conditions to obtain accurate estimations. Low radium levels observed in 2022 suggest that upwelling events can perturb coastal radium levels by transporting SGD-derived radium offshore, and/or by transporting nutrient-rich deeper waters to the surface that enhance primary productivity, potentially increasing coincidental Ra uptake. This study highlights the importance of sampling across different time periods to capture the variability in coastal radium distribution and nutrient transport. Continued monitoring in this area will be useful in determining whether low radium activities align with the timing and spatial extent of upwelling events.

Groundwater serves as a major source of nutrients along this stretch of coast, contributing fluxes on par with the Delaware River Estuary and ~200% higher than those delivered by the nearby Mullica River. These results demonstrate the importance of groundwater as a key nutrient source and provide baseline estimates for assessing the impacts of human activities and sea-level rise on the magnitude and quality of groundwater discharge along the New Jersey coast. Assessing these changes will be crucial in providing local decision-makers with valuable

information regarding pollution management and ensuring the safety of coastal environments and local fisheries. These baselines will enable direct comparisons of SGD before and after wind energy development in New Jersey and offer insight into how similar passive margin coastlines may respond to future offshore wind installations globally.

Data availability statement

Data are available through the Environmental Data Initiative (https://doi.org/10.6073/pasta/58bbe85d494dafc9f8189e207a18b86d).

CRediT authorship contribution statement

Joanna A. Guldin: Data curation, Formal analysis, Investigation, Visualization, Writing – original draft, Writing – review & editing. **Charles A. Schutte:** Conceptualization, Funding acquisition, Investigation, Methodology, Resources, Supervision, Validation, Writing – review & editing. **Lauren E. Kipp:** Conceptualization, Formal analysis, Funding acquisition, Investigation, Methodology, Project administration, Resources, Supervision, Validation, Writing – review & editing.

Declaration of competing interest

The authors declare that they have no known competing financial interests or personal relationships that could have appeared to influence the work reported in this paper.

Acknowledgements

We thank Captain Steve Evert and Stockton University for use of the *R/V Petrel*. We also thank Elizabeth Fuchs, Kriish Hate, Amber Hatter, and Alyssa Robbins for performing sample collection and analysis in 2022, Dr. Beth Christensen for assisting with sample collection in 2022 and 2023, and Jonathan Hansel for his assistance in making Fig. 1. This work was supported by a Rowan University CATALYST grant to L.K., C. S., and B.C.

Appendix A. Supplementary data

Supplementary data to this article can be found online at https://doi.org/10.1016/j.ecss.2026.109766.

References

Barlow, P.M., Reichard, E.G., 2010. Saltwater intrusion in coastal regions of North America. Hydrogeol. J. 18 (1), 247–260. https://doi.org/10.1007/s10040-009-0514-3.

Burnett, W.C., Bokuniewicz, H., Huettel, M., Moore, W.S., Taniguchi, M., 2003. Groundwater and pore water inputs to the coastal zone. Biogeochemistry 66, 3–33. https://doi.org/10.1023/B:BIOG.0000006066.21240.53.

Burnett, W.C., Peterson, R., Moore, W.S., de Oliveira, J., 2008. Radon and radium isotopes as tracers of submarine groundwater discharge - results from the Ubatuba, Brazil SGD assessment intercomparison. Estuar. Coast Shelf Sci. 76 (3), 501–511. https://doi.org/10.1016/j.ecss.2007.07.027.

Charette, M.A., Morris, P.J., Henderson, P.B., Moore, W.S., 2015. Radium isotope distributions during the US GEOTRACES North Atlantic cruises. Mar. Chem. 177, 184–195. https://doi.org/10.1016/j.marchem.2015.01.001.

Delaware River Basin Commission, 2023. Delaware river flow and storage data—June, 2023 [Data set]. https://www.nj.gov/drbc/library/documents/data/june23.pdf.

Diaz, R.J., Rosenberg, R., 2008. Spreading dead zones and consequences for marine ecosystems. Science 321 (5891), 926–929. https://www.jstor.org/stable/20144596.

Fisher, T.R., Gustafson, A.B., 2019. *Report to DRBC on Concentration of Nutrients and Chlorophyll a and Rates of Respiration and Primary Production in Samples from the Delaware River Collected in May and July 2018.* Horn Point Laboratory. University of Maryland.

Fisher, T.R., Gustafson, A.B., 2020. *Report to DRBC on Concentration of Nutrients and Chlorophyll a and Rates of Respiration and Primary Production in Samples from the Delaware River Collected in May and July 2019.* Horn Point Laboratory. University of Maryland.

Garcia-Orellana, J., Rodellas, V., Tamborski, J., Diego-Feliu, M., van Beek, P., Weinstein, Y., Charette, M., Alorda-Kleinglass, A., Michael, H.A., Stieglitz, T., Scholten, J., 2021. Radium isotopes as submarine groundwater discharge (SGD) tracers: review and recommendations. Earth Sci. 220, 103681. https://doi.org/10.1016/j.earscirev.2021.103681.

Glenn, S., Arnone, R., Bergmann, T., Bissett, W.P., Crowley, M., Cullen, J., Gryzmski, J., Haidvogel, D., Kohut, J., Moline, M., Oliver, M., Orrico, C., Sherrell, R., Song, T., Weidemann, A., Chant, R., Schofield, O., 2004. Biogeochemical impact of summertime coastal upwelling on the New Jersey Shelf. J. Geophys. Res., Oceans 109 (C12). https://doi.org/10.1029/2003JC002265, 2003JC002265.

Huh, C.-A., Ku, T.-L., 1998. A 2—D section of 228Ra and 226Ra in the Northeast Pacific. Oceanol. Acta 21 (4), 533–542. https://doi.org/10.1016/S0399-1784(98)80036-4.

Key, R.M., Sarmiento, J.L., Moore, W.S., 1985. Distribution of Ra-228 and Ra-226 in the Atlantic Ocean. Ocean Tracer Lab, Princeton. Technical Report.

Krishnaswami, S., Graustein, W.C., Turekian, K.K., Dowd, J.F., 1982. Radium, thorium and radioactive lead isotopes in groundwaters: application to the in situ determination of adsorption-desorption rate constants and retardation factors. Water Resour. Res. 18 (6), 1663–1675. https://doi.org/10.1029/WR018i006p01663.

Methods for the determination of inorganic substances in environmental samples. EPA 600/R 93/100, 1993. Method 353.2, Revision 2.0.

Methods for the determination of inorganic substances in environmental samples. EPA 600/R 93/100, 1993. Method 350.1, Revision 2.0.

Methods for the determination of inorganic substances in environmental samples. USEPA 600/R 93/100, 1993. Method 365.1, Rev 2.0.

Moline, M.A., Blackwell, S.M., Chant, R., Oliver, M.J., Bergmann, T., Glenn, S., Schofield, O.M.E., 2004. Episodic physical forcing and the structure of phytoplankton communities in the coastal waters of New Jersey. J. Geophys. Res., Oceans 109 (C12). https://doi.org/10.1029/2003JC001985, 2003JC001985.

Moore, W.S., 2010. A reevaluation of submarine groundwater discharge along the southeastern coast of North America. Glob. Biogeochem. Cycles 24 (4). https://doi.org/10.1029/2009GB003747, 2009GB003747.

Moore, W.S., Benitez-Nelson, C., Schutte, C., Moody, A., Shiller, A., Sibert, R.J., Joye, S., 2024. SGD-OD: investigating the potential oxygen demand of submarine groundwater discharge in coastal systems. Sci. Rep. 14 (1), 9249. https://doi.org/10.1038/s41598-024-59229-7.

Moore, W.S., Sarmiento, J.L., Key, R.M., 2008. Submarine groundwater discharge revealed by ^{228}Ra distribution in the upper Atlantic Ocean. Nat. Geosci. 1 (5), 309–311. https://doi.org/10.1038/ngeo183.

Moore, W.S., 2000a. Ages of continental shelf waters determined from ^{223}Ra and ^{224}Ra. J. Geophys. Res., Oceans 105 (C9), 22117–22122. https://doi.org/10.1029/1999JC000289.

Moore, W.S., Arnold, R., 1996. Measurement of ^{223}Ra and ^{224}Ra in coastal waters using a delayed coincidence counter. J. Geophys. Res. 101 (C1), 1321–1329. https://doi.org/10.1029/95JC03139.

Moore, W.S., Cai, P., 2013. Calibration of RaDeCC systems for ^{223}Ra measurements. Mar. Chem. 156, 130–137. https://doi.org/10.1016/j.marchem.2013.03.002.

Moore, W.S., Joye, S.B., 2021. Saltwater intrusion and submarine groundwater discharge: acceleration of biogeochemical reactions in changing coastal aquifers. Front. Earth Sci. 9, 600710. https://doi.org/10.3389/feart.2021.600710.

Moore, W.S., 2000b. Determining coastal mixing rates using radium isotopes. Cont. Shelf Res. 20 (15), 1993–2007. https://doi.org/10.1016/S0278-4343(00)00054-6.

Moosdorf, N., Oehler, T., 2017. Societal use of fresh submarine groundwater discharge: an overlooked water resource. Earth Sci. Rev. 171, 338–348. https://doi.org/10.1016/j.earscirev.2017.06.006.

New Jersey Board of Public Utilities, 2020. 2019 New Jersey energy master plan: pathway to 2050. https://www.nj.gov/emp/docs/.

NJDEP Bureau of Marine Water Monitoring, 2020. Nutrient monitoring results [Data set]. https://dep.nj.gov/wms/bmw/data/.

NOAA's National Ocean Service. *Station ACYN4 – 8534720 – Atlantic City, NJ.* National data buoy center. https://www.ndbc.noaa.gov/station_page.php?station=acyn4.

Paerl, H.W., 1997. Coastal eutrophication and harmful algal blooms: importance of atmospheric deposition and groundwater as "new" nitrogen and other nutrient sources. Limnol. Oceanogr. 42, 1154–1165. https://doi.org/10.4319/lo.1997.42.5_part_2.1154.

Rama, Moore, W.S., 1996. Using the radium quartet for evaluating groundwater input and water exchange in salt marshes. Geochem. Cosmochim. Acta 60 (23), 4645–4652. https://doi.org/10.1016/S0016-7037(96)00289-X.

Reid, D.F., Key, R.M., Schink, D.R., 1979. Radium, thorium, and actinium extraction from seawater using an improved manganese-oxide-coated fiber. Earth Planet Sci. Lett. 43 (2), 223–226. https://doi.org/10.1016/0012-821X(79)90205-X.

Santos, I.R., Burnett, W.C., Chanton, J., Mwashote, B., Suryaputra, I.G.N.A., Dittmar, T., 2008. Nutrient biogeochemistry in a Gulf of Mexico subterranean estuary and groundwater-derived fluxes to the coastal ocean. Limnol. Oceanogr. 53. https://doi.org/10.4319/lo.2008.53.2.0705.

Santos, I.R., Chen, X., Lecher, A.L., Sawyer, A.H., Moosdorf, N., Rodellas, V., Tamborski, J., Cho, H.-M., Dimova, N., Sugimoto, R., Bonaglia, S., Li, H., Hajati, M.-C., Li, L., 2021. Submarine groundwater discharge impacts on coastal nutrient biogeochemistry. Nat. Rev. Earth Environ. 2 (5), 307–323. https://doi.org/10.1038/s43017-021-00152-0.

Sawyer, A.H., David, C.H., Famiglietti, J.S., 2016. Continental patterns of submarine groundwater discharge reveal coastal vulnerabilities. Science 353, 705–707. https://doi.org/10.1126/science.aag1058.

Schultze, L.K.P., Merckelbach, L.M., Horstmann, J., Raasch, S., Carpenter, J.R., 2020. Increased mixing and turbulence in the wake of offshore wind farm foundations. J. Geophys. Res., Oceans 125 (8). https://doi.org/10.1029/2019JC015858 e2019JC015858.

Stachelhaus, S.L., Moran, S.B., Ullman, D.S., Kelly, R.P., 2012. Cross-shelf mixing and mid-shelf front dynamics in the Mid-Atlantic Bight evaluated using the radium quartet. J. Mar. Res. 70 (1). https://elischolar.library.yale.edu/journal_of_marine_research/336.

USGS. Mullica river near Batsto NJ – 01409400. https://waterdata.usgs.gov/monitoring-location/01409400/.

Valiela, I., Costa, J., Foreman, K., Teal, J.M., Howes, B., Aubrey, D., 1990. Transport of groundwater-borne nutrients from watersheds and their effects on coastal waters. Biogeochemistry 10 (3), 177–197. https://doi.org/10.1007/BF00003143.

van Beek, P., François, R., Honda, M., Charette, M.A., Reyss, J.-L., Ganeshram, R., Monnin, C., Honjo, S., 2022. Fractionation of ^{226}Ra and Ba in the Upper North Pacific Ocean. Front. Mar. Sci. 9, 859117. https://doi.org/10.3389/fmars.2022.859117.